Vanadium(V) Oxo and Imido calix[8]arene complexes: Synthesis, structural studies and ethylene homo-(co-)polymerization capability.

Carl Redshaw,[a,*] Mark J. Walton,[b] Darren S. Lee,[c] Chengying Jiang,[c] and Mark R.J. Elsegood[c] and Kenji Michiue [d]

[a] *Department of Chemistry, University of Hull, Hull, HU6 7RX, U.K.*

[b] *Energy Materials Laboratory, School of Chemistry, University of East Anglia, Norwich, NR4 7TJ, U.K.*

[c] *Chemistry Department, Loughborough University, Loughborough, Leicestershire, LE11 3TU,U.K.*

[d] *Process Technology Center, Mitsui Chemicals Inc., 580-32 Nagaura, Sodegaura, Chiba 299-0265, Japan*

Abstract: Interaction of p-*tert*-butylcalix[8]areneH_8 (L^8H_8) with *in-situ* generated [NaVO(O*t*-Bu)$_4$] (from $VOCl_3$ and four equivalents of NaO*t*Bu) afforded the dark brown complex $[Na(NCMe)_5][(VO)_2L^8H]\cdot 4MeCN$ (**1**·4MeCN), in which the calix[8]arene adopts a saddle-shaped conformation. Increasing (to four equivalents per L^8) the amount of [NaVO(O*t*-Bu)$_4$] present in the reaction, led to the formation of the yellow octa-vanadyl complex $\{[(Na(VO)_4L^8)(Na(NCMe))_3][Na(NCMe)_6\}_2\cdot 10MeCN$ (**2**·10MeCN), in which the calix[8]arene adopts a pleated loop conformation. In the presence of adventitious oxygen, reaction of four equivalents of [VO(O*t*-Bu)$_3$] (generated from $VOCl_3$ and 3KO*t*Bu) with L^8H_8 afforded the alkali-metal free green complex $[(VO)_4L^8(\mu^3\text{-}O)_2]$ (**3**); the solvates **3**·3MeCN and **3**·3CH_2Cl_2 have been isolated. In both solvates, the L^8 ligand adopts a shallow saddle-shaped conformation, supporting a core comprising of a $(VO)_4O_4$ ladder. In the case of lithium, in order to obtain crystalline material, it was found necessary to reverse the order of addition such that lithium *tert*-butoxide

was added to L^8H_8, and then subsequently treated (at –78 ^oC) with two equivalents of $VOCl_3$; crystallization from tetrahydrofuran (THF) afforded $\{(VO_2)_2Li_6[L^8](thf)_2(OtBu)_2(Et_2O)_2\}\cdot Et_2O$ (**4**·Et_2O). In the structure of **4**·Et_2O, vanadium, lithium and oxygen form a central lattern-type cage, which is capped top and bottom by an Li_2O_2 diamond; the calix[8]arene is in a 'down, down, out, out, down, down' conformation. When the 'same reaction' was extracted into acetonitrile (MeCN), the salt complex $[Li(NCMe)_4][(VO)_2L^8H]\cdot 8MeCN$ (**5**·8MeCN) was formed. In **5**·8MeCN, the $[Li(NCMe)_4]$ cations reside between the anions in the clefts of L^8H, the latter adopting a saddle-shaped conformation. Use of the imido precursors [V(N*t*-Bu)(O*t*-Bu)$_3$] and [V(N*p*-tolyl)(O*t*-Bu)$_3$] and L^8H_8, afforded, via an imido exchange, the salt $[t\text{-}BuNH_3]\{[V(p\text{-}tolylN)]_2L^8H\}\cdot 3½MeCN$ (**6**·3½MeCN). The molecular structures of **1** to **6** are reported; data collections for complexes **2**·10MeCN, **3**·3MeCN and **3**·$3CH_2Cl_2$ required the use of synchrotron radiation. Complexes **1, 3** and **4** have been screened as pre-catalysts for the polymerization of ethylene in the presence of a variety of co-catalysts (with and without a re-activator) at various tempertures and for the co-polymerization of ethylene with propylene; results are compared *versus* the benchmark catalyst $VO(OEt)Cl_2$. In some cases, activities as high as 136,000 g/mmol.v.h were achievable, whilst it also proved possible to obtain higher molecular weight polymers (in comparible yields) *versus* the use of $VO(OEt)Cl_2$. In the case of the co-polymerization, the incorporation of propylene was 7.1 – 10.9 mol% (*cf* 10 mol% for $VO(OEt)Cl_2$), though catalytic activities were lower *versus* $VO(OEt)Cl_2$.

Keywords: Vanadium; calix[8]arene; ethylene polymerization; ethylene/propylene co-polymerization; crystal structures.

Introduction

The use of calix[*n*]arenes in a variety of catalytic/polymerization processes continues to attract interest. [1] However, the majority of the work in the literature has focussed on systems employing the 'simplest' of the calixarene family, p-*tert*-butylcalix[4]areneH_4, partly due to its ease of preparation (low cost), but also given the calix[4]arene ligand set tends to bind to only one metal, retaining a cone conformation, thereby making characterization relatively simple. Furthermore, Floriani recognized that the calix[4]arene ligand system, with the four oxygen donors of the lower-rim, was pre-organized in a quasi-planar geometry, and offered an ideal opportunity for modelling an oxo surface and thereby heterogeneous catalysts. [2] By contrast, the coordination chemistry associated with the larger calix[*n*]arenes (n > 4) is less well studied, [3, 4] presumably reflecting the often increased costs associated with the preparation of these larger ligands, as well as the more complicated characterization necessary for resulting larger metallocalix[*n*]arenes. However, there are advantages for targeting larger metallocalix[*n*]arenes, for example their increased conformational flexibility, presence of multiple cavities and their ability to coordinate simultaneously multiple metal centres, means that such systems are becoming of increased structural interest. With respect to catalysis, the ability to coordinate multiple metal centres in close proximity has the potential to lead to useful cooperative effects. [5] With this in mind, we now describe the synthesis and solid-state structures of a number of new vanadium(V) p-*tert*-butylcalix[8]arene complexes (chart 1), noting that structural reports of vanadium complexes of the larger calix[*n*]arenes remain scant. [3, 6, 7] In the case of vanadium-based calixarene catalysis, Limberg *et al* have screened such systems for the oxidative dehydrogenation of short chain alkanes and alcohols, [6] whilst our group has screened a range of vanadyl-containing calix[*n*]arenes for α-olefin homo-(co-)polymerization. [7] We have also described the difficulties associated with the use of alkali metal alkoxides, and the resulting structural complications for a

number of chromium(III) and iron(III) complexes bearing p-*tert*-butylcalix[4 and 6]arenes. [8, 9] Herein, similar use of alkali metal alkoxides also leads to some intriguing p-*tert*-butylcalix[8]arene structures, and, given the current interest in the potential of vanadium-based systems for olefin polymerization, a number of the vanadyl complexes prepared herein have been screened for their ability to polymerize ethylene and co-polymerize ethylene with propylene. The use of different co-catalysts is evaluated as is the variation of temperature on the catalytic performance**;** results are compared *versus* the benchmark catalyst $VO(OEt)Cl_2$. We note that our recent studies using vanadyl p-*tert*-butylcalix[6]arene complexes revealed that activities as high as 202,500 g/mmol.v.h were achievable, although such systems suffered somewhat from thermal instability. [10]

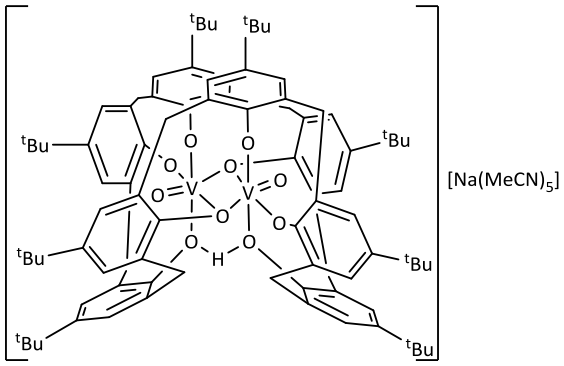

1

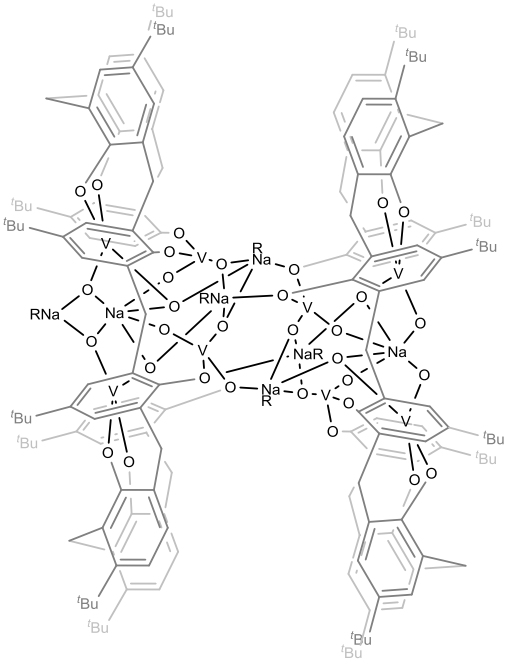

2 (R = MeCN)

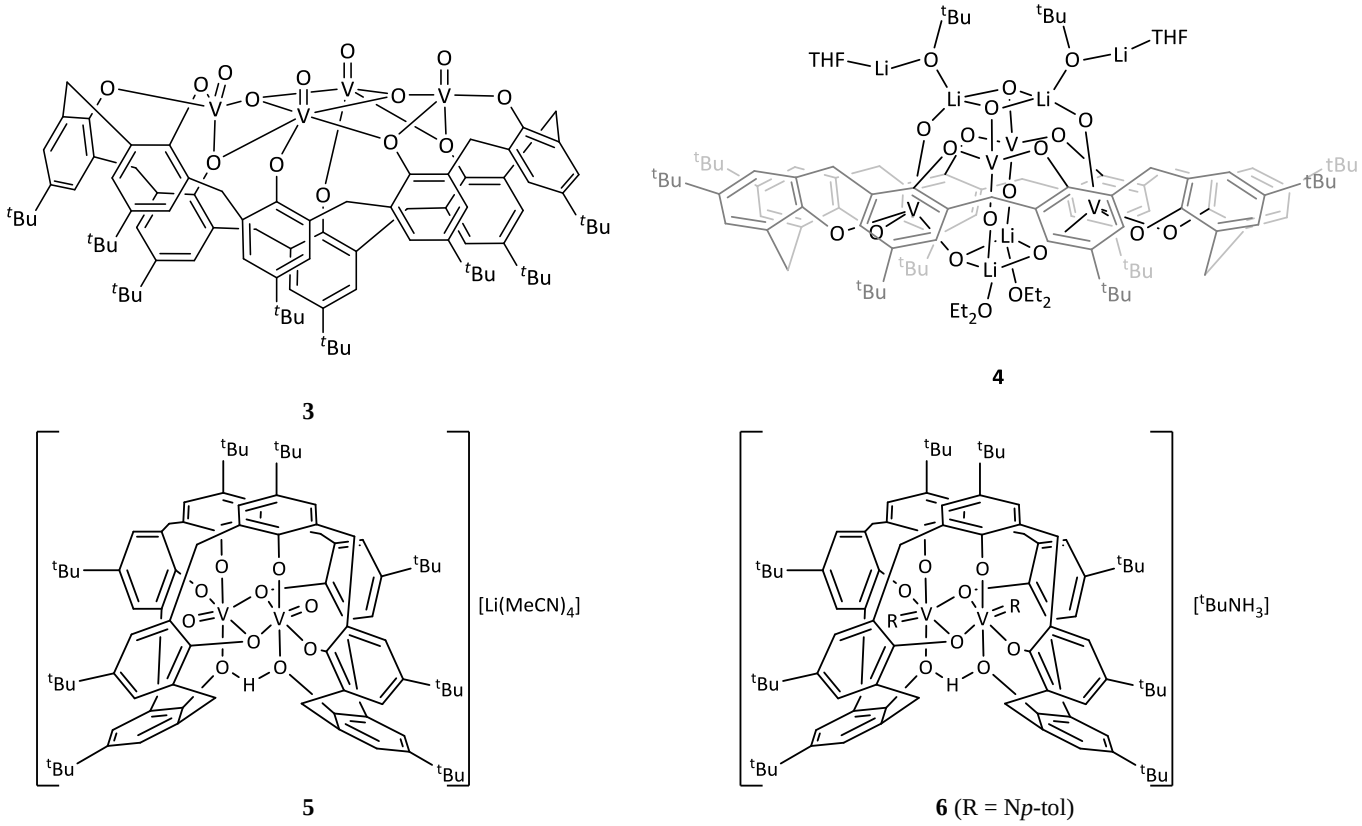

Chart 1. Vanadium calix[8]arenes prepared in this work.

Results and Discussion

'Vanadyl sodium' complexes

Interaction of p-*tert*-butylcalix[8]areneH_8 (L^8H_8) with [NaVO(O*t*-Bu)$_4$] (prepared *in-situ* from $VOCl_3$ and excess NaO*t*Bu using a modification of the method of Wilkinson [11]) afforded the dark brown complex $[Na(NCMe)_5][(VO)_2L^8H]\cdot 5MeCN\cdot$(**1**$\cdot$4MeCN), in *ca*. 47 % yield. Crystals of **1**·4MeCN suitable for single crystal X-ray diffraction studies were grown from saturated acetonitrile solutions after prolonged standing at ambient temperature. The molecular structure of complex **1** is presented in Figure 1; crystallographic data are collated in Table 6. The structure of this salt is similar to those previously reported by Pedersen *et al* and by Limberg *et al*, who prepared ammonium and phosphonium salts, respectively. [6, 12] As shown in Figure 2, the calix[8]arene adopts a saddle-

shaped conformation, which creates two small cavities, each comprising three phenolic groups, at each 'end' of the complex. One oxygen [O(5)] remains protonated and forms a hydrogen bond with O(1). The geometry at each vanadium centre is best described as pseudo octahedral, and these vanadium centres are linked via asymmetric aryloxide bridges, with the longer bridging bond lying *trans* to the oxo function. Selected structural parameters for **1** and those of the 'Limberg structure' (CCDC 610228) are compared in Table 1; the 'Pedersen structure' was not characterized crystallographically (rather it was inferred by NMR spectroscopic data and by comparison with a crystallographically characterized titanium complex of L^8H). As expected, there is good agreement between the geometrical parameters for each structure, for example terminal V=O bonds lengths 1.589(2) and 1.591(2) Å in **1** compare favourably with those reported by Limberg [1.589(2) and 1.599(2) Å]. The sodium cation in **1** is bound by five acetonitrile molecules.

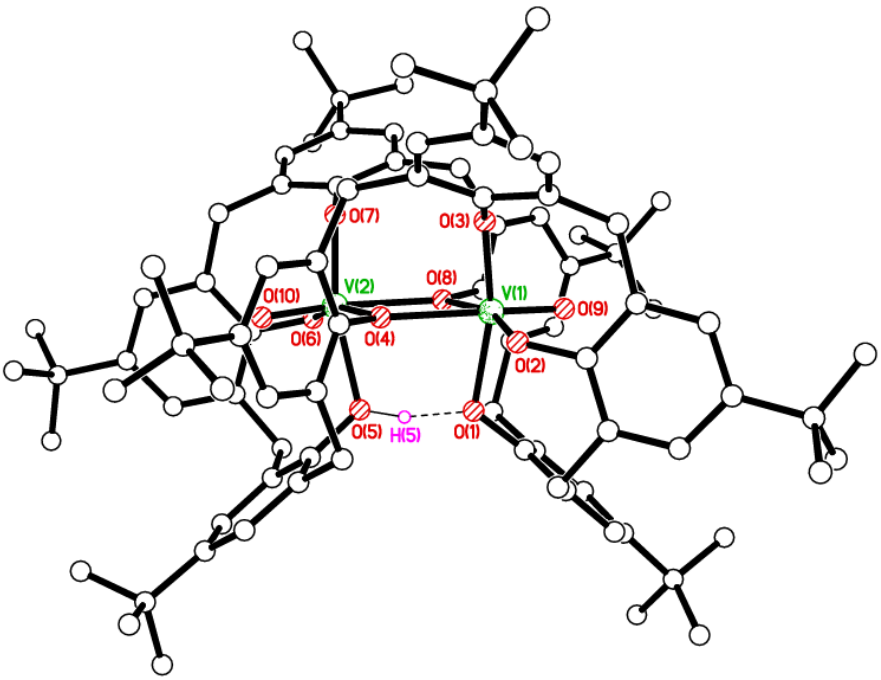

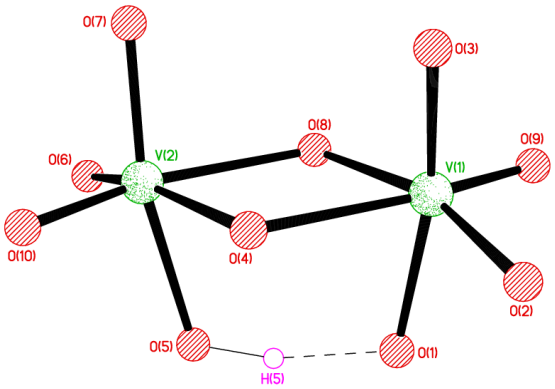

Figure 1. Top: view of **1** showing the atom numbering scheme and revealing the saddle-shaped geometry of L^8H. H atoms except H(5), the $[Na(NCMe)_5]^+$ cation, and five MeCN molecules of crystallisation are omitted for clarity. Below: the core of **1**.

Table 1. Selected structural data for **1** and Limberg salt $[PPh_4][(VO)_2L^8H]$

Bond length (Å)/Angle (°)	**1**	Limberg salt
V(1)-O(1)	2.0148(19)	2.036(2)
V(1)-O(2)	1.8452(19)	1.849(2)
V(1)-O(3)	1.855(2)	1.852(2)
V(1)-O(4)	2.181(2)	2.212(2)
V(1)-O(8)	1.9916(19)	1.992(2)
V(1)-O(9)	1.589(2)	1.589(2)
V(1)···V(2)[a]	3.3695(7)	3.3677(7)
O(1)-V(1)-O(3)	163.56(9)	162.87(8)
O(4)-V(1)-O(8)	72.11(7)	71.89(6)
O(4)-V(1)-O(9)	165.81(9)	164.44(8)
V(1)-O(4)-V(2)	108.33(9)	107.20(8)
V(1)-O(8)-V(2)	107.28(8)	107.77(8)

[a]Not bonded.

Increasing the amount of $[NaVO(O\textit{t}\text{-}Bu)_4]$ present in the reaction to four equivalents, led to the formation of $\{[(Na(VO)_4L^8)(Na(NCMe))_3][Na(NCMe)_6]\}_2 \cdot 10MeCN$ (**2**·10MeCN). Small crystals of

2·10MeCN suitable for single crystal X-ray diffraction studies using synchrotron radiation were grown from saturated acetonitrile solutions after prolonged standing at –25 °C. A view of the molecular structure of compound **2** is presented in Figures 2, together with a picture of the core; selected bond lengths and angles are given in the caption.

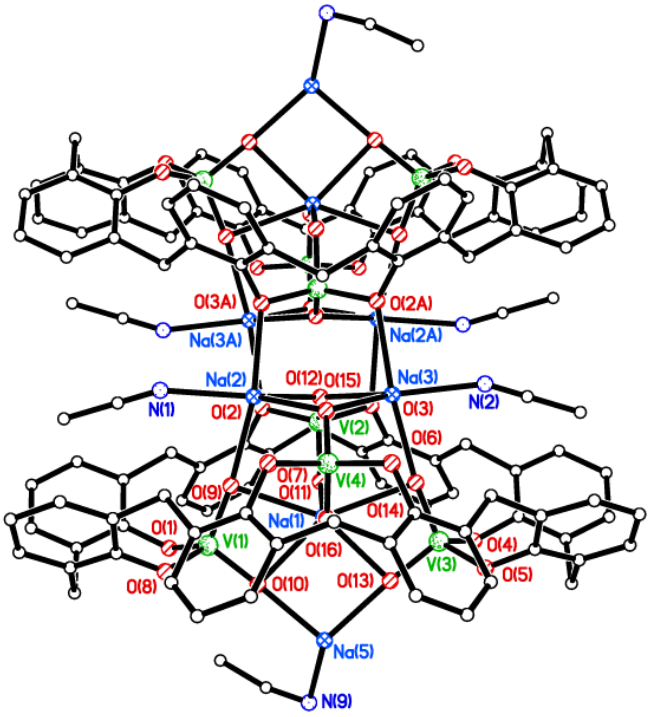

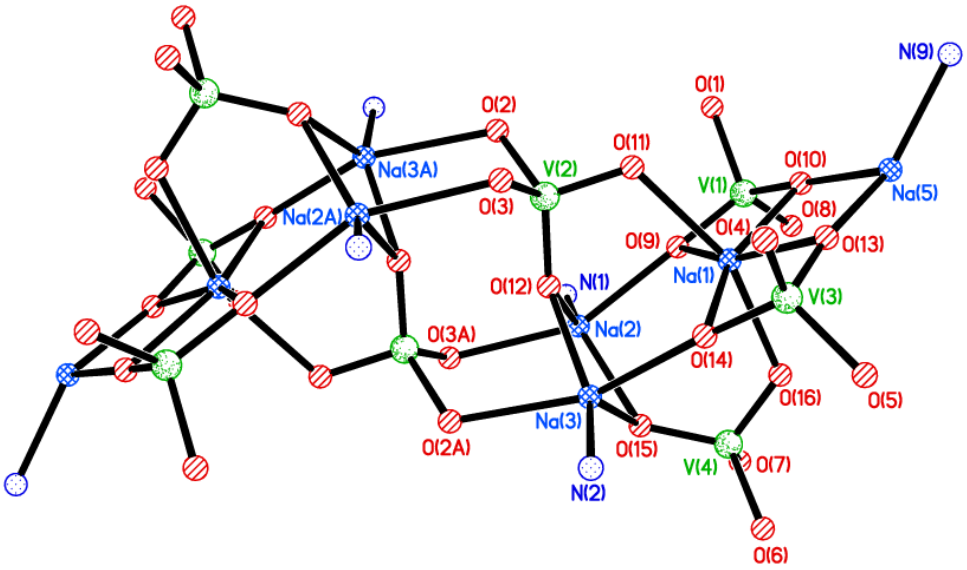

Figure 2. Top: view of the anion in **2**. Hydrogen atoms, *tert*-butyl groups on the calixarene and non-coordinated solvent molecules have been omitted for clarity. Note: Na(5) and the attached MeCN are 50 % occupied, i.e. on average, only one of these groups per anion. Below: the core of **2**. Selected bond lengths (Å) and angles (^{o}): V(1) – O(1) 1.810(5), V(1) – O(8) 1.824(5), V(1) – O(9) 1.646(5), V(1) – O(10) 1.630(5), V(2) – O(2) 1.846(4), V(2) – O(3) 1.841(4), V(2) – O(11) 1.597(5), V(2) – O(12) 1.670(4), V(3) – O(4) 1.802(5), V(3) – O(5) 1.813(5), V(3) – O(13) 1.619(5), V(3) – O(14) 1.646(4), V(4) – O(6) 1.826(5), V(4) – O(7) 1.818(5), V(4) – O(15) 1.649(4), Na – O range 2.24-2.51(2); O(1) – V(1) – O(8) 105.4(2), O(1) – V(1) – O(9) 112.7(2), O(8) – V(1) – O(9) 113.2(2), O(2) – V(2) – O(3) 106.21(18), O(2) – V(2) – O(12) 116.2(2), O(4) – V(3) – O(5) 105.1(2), O(4) – V(3) – O(14) 112.4(2), O(6) – V(4) – O(7) 106.8(2), O(6) – V(4) – O(15) 111.6(2).

The molecule is located on an inversion centre, with each half containing four VO_2 units, surrounding a six-coordinate sodium cation, Na(1). The two halves of the molecule are linked via a central $V_2Na_2O_4$ unit. The L^8 ligand forms a 'pleated-loop' conformation. Four sodium cations (two unique) reside within the framework connecting the two calixarenes and are each bound by one solvent molecule. At one end of the molecule or the other, but not both, is a further Na(NCMe) group, containing Na(5), highlighting the ability of such systems to pick up solvated alkali metals at any exposed oxygen sites. A further sodium per asymmetric unit is present, and this is bound by six acetonitriles, and acts as a separate cationic unit.

'Vanadyl potassium' complexes

By contrast, in the presence of adventitious oxygen, the use of four equivalents [VO(O*t*-Bu)$_3$] (generated *in-situ* from [$VOCl_3$] and 3KO*t*Bu) and L^8H_8 afforded the alkali-metal free, green complex

$[(VO)_4L^8(\mu^3\text{-}O)_2]$ (**3**). Two solvates, namely **3**·3MeCN and **3**·$3CH_2Cl_2$ have been isolated from work-ups involving either acetonitrile or dichloromethane, respectively, and structurally characterized. Diffraction data for both solvates of **3** were collected using synchrotron radiation. They are isomorphous and both are twinned (see experimental section).

Views of two solvates, **3**·3MeCN and **3**·$3CH_2Cl_2$ are presented in Figure 3. In both molecules, the geometry around each vanadium centre is very similar (square-pyramidal), reflected by the near identical bond lengths and angles – see Table 2. Each molecule lies on a centre of inversion.

Table 2. Selected structural data for the solvates **3**·3MeCN and **3**·$3CH_2Cl_2$.

Bond lengths (Å)/Angle (°)	**3**·3MeCN	**3**·$3CH_2Cl_2$
V(1)-O(3)	1.914(5)	1.914(3)
V(1)-O(4)	1.776(6)	1.762(3)
V(1)-O(10)	1.572(6)	1.573(3)
V(1)-O(13)	1.946(6)	1.939(3)
V(1)-O(14)	1.931(5)	1.949(3)
V(3)-O(1)	1.799(6)	1.798(3)
V(3)-O(2)	1.786(6)	1.788(2)
V(3)-O(3)	2.214(6)	2.200(3)
V(3)-O(9)	1.562(6)	1.580(3)
V(3)-O(13)	1.878(5)	1.884(3)
V(1)-O(3)-V(3)	98.7(2)	97.56(12)
V(1)-O(13)-V(3)	110.3(3)	108.36(14)
V(1)-O(13)-V(2)	103.2(2)	104.62(13)
V(1)-O(14)-V(4)	145.2(3)	143.97(17)

The two fully deprotonated calix[8]arene moieties each adopt a shallow, saddle-shaped conformation and chelate to four penta-coordinated vanadyl centres. The vanadium and oxygen atoms are arranged

in a ladder-like configuration (Figure 3, top), similar to that reported for a number of titanium based calixarene complexes, for example **I** and more recently for the iron(III) calix[6]arene complex [{Fe_2(μ-O)L^6(K(NCMe)$_2$)$_2$}$_2$]·10.8MeCN **II** (see Chart 2), [9]

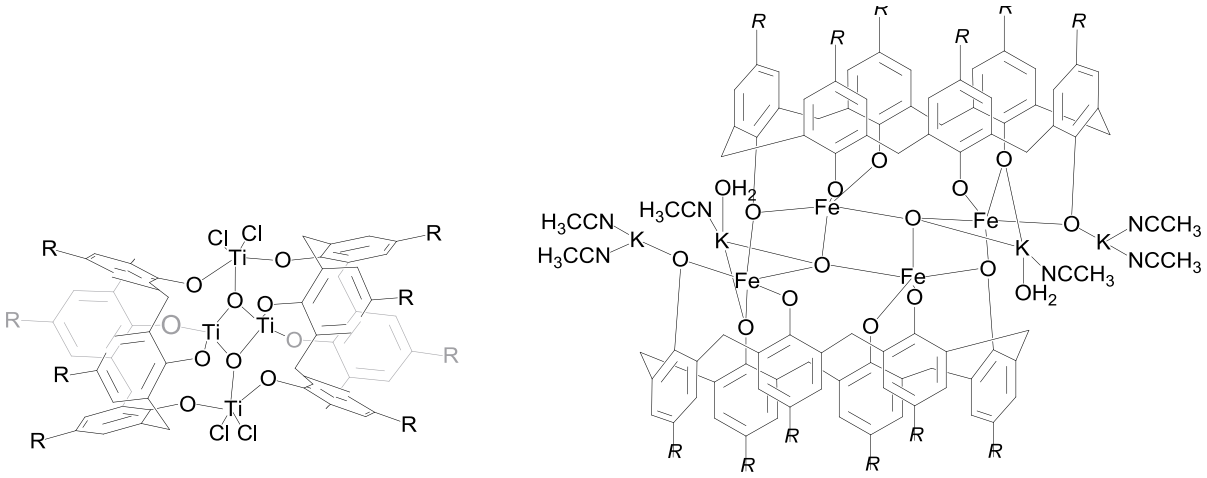

Chart 2

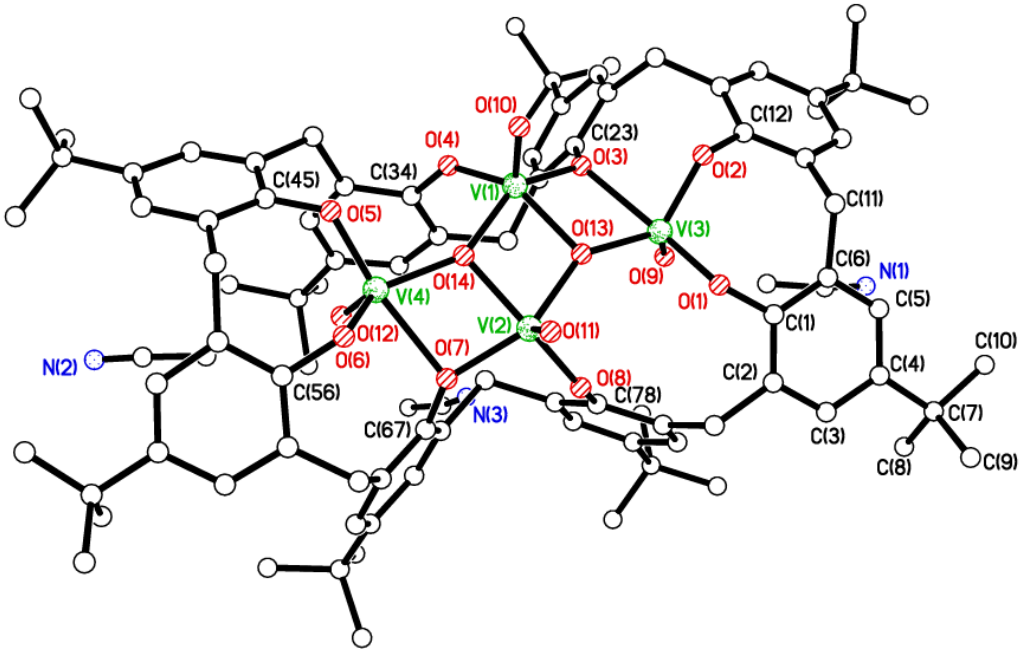

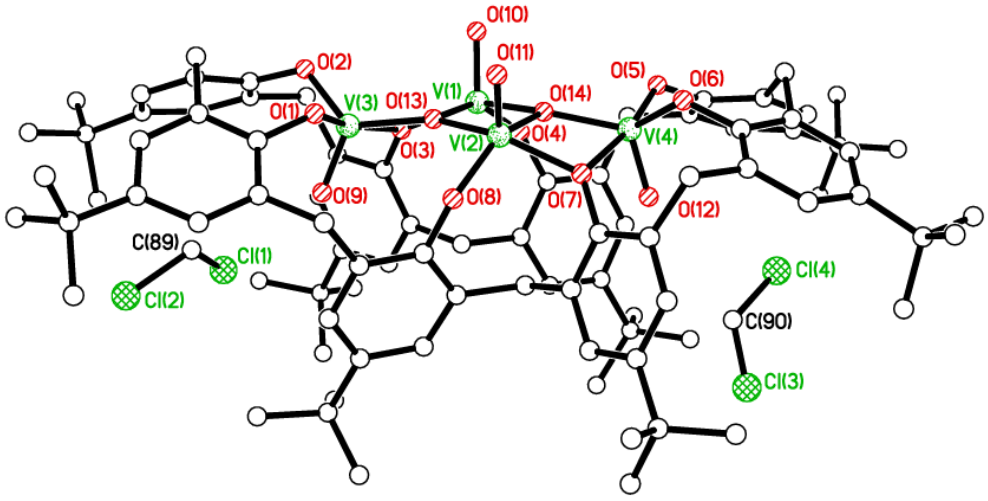

Figure 3–Views of the two solvates, **3**·3MeCN (top) and **3**·3CH_2Cl_2 (bottom). Hydrogen atoms have been omitted for clarity. Top: this view highlights the V_4O_4 ladder in the core; below: this view shows two of the three solvent molecules encapsulated by the calixarene, one at each end of the molecule.

'Vanadyl lithium' complexes

In the case of lithium, in order to obtain crystalline material, it was necessary to reverse the order of addition such that lithium *tert*-butoxide was added to L^8H_8, and subsequently treated (at –78 ^oC) with two equivalents of $VOCl_3$; crystallization from tetrahydrofuran (THF) afforded $\{(VO_2)_2Li_6[L^8](thf)_2(O\mathit{t}Bu)_2(Et_2O)_2\}\cdot Et_2O$ (**4**·Et_2O). Two views of the molecular structure of compound **4** are presented in Figures 4a and 4b, together with a picture of the core (Figure 5); selected bond lengths and angles are given in the caption.

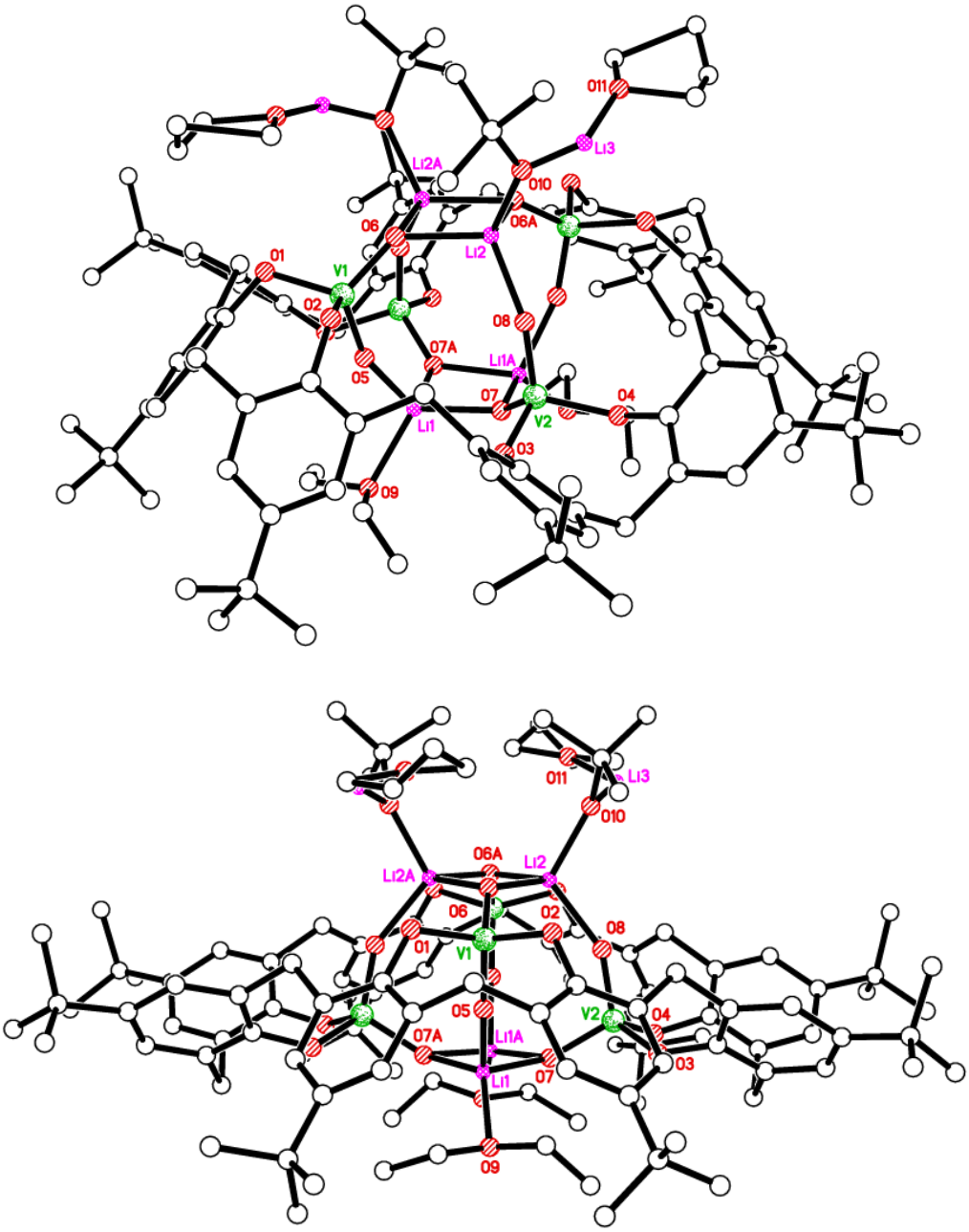

Figure 4. Two views of the complex **4**·Et_2O. Selected bond lengths (Å) and angles (°): V(1) – O(1) 1.825(3), V(1) – O(2) 1.821(3), V(1) – O(5) 1.618(3), V(1) – O(6) 1.665(3), V(2) – O(3) 1.795(3), V(2) – O(4) 1.797(3), V(2) – O(7) 1.660(3), V(2) – O(8) 1.624(3), Li(1) – O(5) 1.930(7), Li(1) – O(7) 1.962(7), Li(1) – O(7A) 1.950(8), Li(1) – O(9) 1.980(8); O(1) – V(1) – O(2) 107.80(12), O(5) – V(1) –

O(6) 110.17(13), O(3) – V(2) – O(4) 105.35(12), O(7) – V(2) – O(8) 111.78(13), O(5) – Li(1) – O(7) 109.8(3).

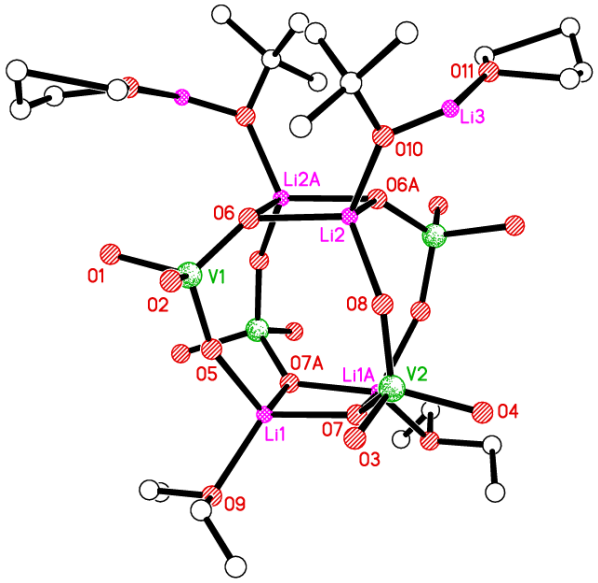

Figure 5. Core of the complex **4**·Et_2O.

The molecule **4**·Et_2O lies on a 2-fold axis, so only half is unique. The calixarene is in the 'down, down, out, out, down, down, out, out' conformation. The lithium centres Li(1) and Li(2) have four bonds which connect with oxygens of the calixarene, vanadyl-O and *tert*-butoxide or Et_2O. Each vanadium centre also connects to four oxygens, and together they construct a lantern shape with Li_2O_2 diamonds top and bottom and four eight-membered panels around the sides. Li(3) makes two bonds which connect with oxygens of thf and a *tert*-butoxide. In terms of the charge balance, there are 8 x O^- on calixarene, 2 x O^- *tert*-butoxides, 8 x O^{2-} as bridging, as well as 4 x V^{5+} and 6 x Li^+.

The data suggest that Li(3) may be replaced by an H atom which would form an H-bond to O(11), thereby making this a *t*BuOH ligand. In reality, this is likely to be a disordered mixture of Li^+ and H^+ as the O–X bond length was too long for H^+ yet too short for Li^+. However, the degree of disorder here

made developing a stable model with so few electrons impossible. The charge balance would then be: 8 x O^{-} on calixarene, 8 x O^{2-} as bridging, and 4 x V^{5+}, 4 x Li^{+}.

When the 'same reaction' was extracted into acetonitrile (MeCN), the salt complex $[Li(NCMe)_4][(VO)_2L^8H]\cdot 8MeCN$ (**5**·8MeCN) was isolated. The molecular structure of **5**·8MeCN is shown in Figure 6, with selected bond lengths and angles given in the caption. The $Li(NCMe)_4]^{+}$ cation resides between pairs of anions, lodged in clefts of the calixarene L^8H. These cation/anion/cation/anion chains align parallel to *b* (see ESI). The MeCN molecules of crystallization also predominantly reside in calixarene clefts.

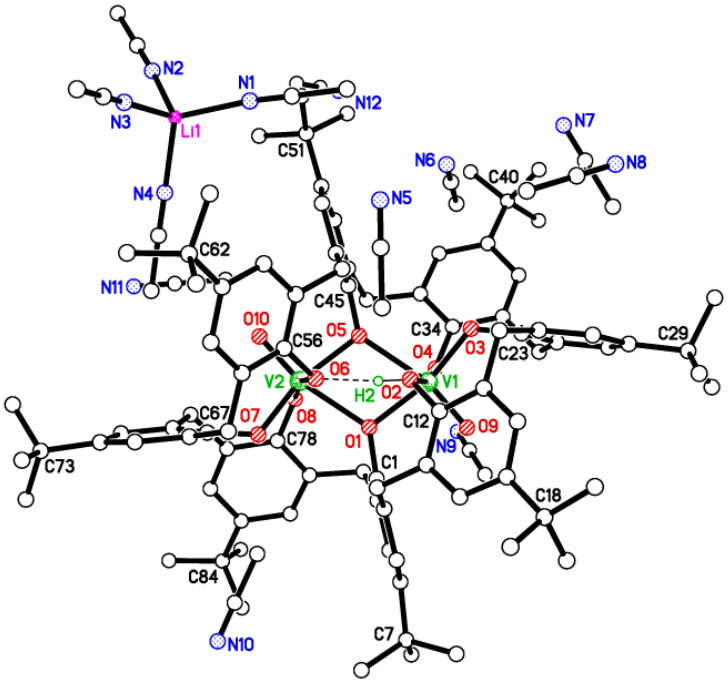

Figure 6. Structure of the salt **5**·8MeCN. V(1) – O(1) 1.967(2), V(1) – O(2) 2.095(2), V(1) – O(3) 1.855(2), V(1) – O(4) 1.840(2), V(1) – O(5) 2.205(2); V(1) – O(1) – V(2) 108.78(10), O(1) – V(1) – O(2) 81.76(10), O(1) – V(1) – O(5) 71.38(9) .

Imido complex:

Use of the imido precursors [V(N*t*-Bu)(O*t*-Bu)$_3$] and [V(N*p*-tolyl)(O*t*-Bu)$_3$] in a 1:1 ratio with L^8H_8, afforded, via imido exchange, the orange/brown salt [*t*-BuNH$_3$]{[V(*p*-tolylN)]$_2L^8H$}·3½MeCN (**6**). Crystals of **6**·3½MeCN suitable for single crystal X-ray diffraction studies were grown from saturated acetonitrile solutions after prolonged standing at –25 °C. The molecular structure of **7** is presented in Figure 7; selected bond lengths and angles are given in Table 3, and are compared with the related complex [V$_2$(N*p*-tolyl)$_2$(H_2L^8)]·4½MeCN. [7a] The anion of **7** adopts a similar local confacial bioctahedral geometry about the two vanadium centres, the latter being linked via asymmetric phenoxide bridges. The calix[8]arene twists such that two sets of three phenoxide subunits each form a small cup and encapsulate an imido group (as highlighted in Figure 7). The [*t*-BuNH$_3$]$^+$ cation is involved in H-bonding with the calixarene phenoxide oxygen O(2) [O(2)···N(3) = 2.737(5) Å, O(2)···H(3A) – N(3) = 175 ^{o}].

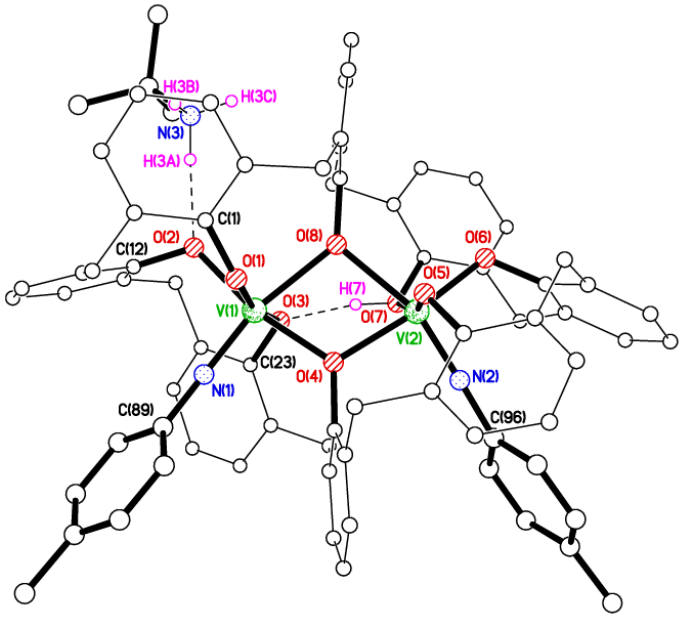

Figure 7. Structure of the salt **6** showing the V_2O_2 core and imido groups each encapsulated by three calixarene phenoxide moieties. Hydrogen atoms, except those involved in H-bonding, *tert*-butyl groups on the calixarene and non-coordinated solvent molecules have been omitted for clarity.

Table 3. Selected structural data for **6** and $[V_2(N\textit{p}\text{-tolyl})_2(H_2L^8)]\cdot 4½MeCN$

Bond length (Å)/Angle (°)	**6**	$[V_2(N\textit{p}\text{-tolyl})_2(H_2L^8)]\cdot 4½MeCN$
V(1)-O(1)	1.896(4)	1.890(2)
V(1)-O(2)	1.922(3)	1.855(2)
V(1)-O(3)	1.981(4)	2.057(2)
V(1)-O(4)	1.962(3)	2.002(2)
V(1)-O(8)	2.162(4)	2.156(2)
V(1)-N(1)	1.672(4)	1.669(3)
V(2)-N(2)	1.670(4)	1.667(3)
V(1)-V(2)	3.3366(13)	3.334
V(1)-O(1)-C(1)	129.6(3)	126.7(2)
V(1)-O(2)-C(12)	119.7(3)	122.90(19)
V(1)-O(3)-C(23)	118.4(3)	120.43(19)
V(1)-O(4)-V(2)	114.38(16)	106.31(10)
V(1)-O(8)-V(2)	101.38(14)	107.12(19)
V(1)-N(1)-C(89)	172.0(4)	175.0(3)
V(1)-N(2)-C(96)	177.7(4)	175.0(3)

Catalytic screening

Ethylene

The complexes **1, 3** and **4** have been screened for their ability to polymerize ethylene in the presence of organoaluminium co-catalysts, namely dimethylaluminium chloride (DMAC) and diethylaluminium

chloride (DEAC), Me_3Al (TMA), Et_3Al (TEA) and dried MAO (DMAO), with or without the re-activating substance ethyltrichloroacetate (ETA) present.

The results are presented in Table 4 and Figure 8, and are further displayed graphically in the ESI (ethylene uptakes). As for other vanadium-based systems, the re-activator ETA is required for high activity. Indeed, it was observed that increasing the amounts of both co-catalyst and ETA present from 5000 Al:5000 ETA to 20000 Al:20000 ETA led to further increased activity. However, the alkylated reagents TMA, TEA and DMAO did not function as co-catalysts. The molecular weights (M_w) of the polyethylene products isolated were mostly high; but PDIs (M_w/M_n) of polyethylene products obtained with DEAC/ETA activation at above 80 ^oC became higher than those with DMAC/ETA.

Variation of temperature

For complex **1**, using Me_2AlCl (DMAC) as co-catalyst (Al/V = 20,000) and in the presence of ethyltrichloroacetate (ETA), the activity peaked at 80 ^oC (163,000 g/mmolV.h), whilst further increases in the temperature resulted in a dramatic fall in activity (down to *ca.* 27,000 g/mmolV.h at 110 ^oC) and complete inactivity at 140 ^oC. As noted for other V-based systems, the molecular weight dropped off rapidly on increasing the temperature, although interestingly the PDI (M_w/M_n) became narrower (tending towards 2.0 at 110 ^oC), suggesting formation of the most stable active species is promoted. On changing the co-catalyst to diethylaluminium chloride (DEAC), the activity peaks (*ca.* 73,000 g/mmolV.h) at the lower temperature of 50 ^oC and rapidly drops off on further increasing the temperature. The polymer molecular weight (M_w) also reduced in value from about 554,000 down to 111,000 over the temperature range 50 to 110 ^oC. Interestingly, in contrast to the behavior by DMAC/ETA activation, the PDI increased from 4.8 at 50 ^oC to over 25.6 at 80 ^oC, suggesting that multiple centres were active at such higher temperatures.

Under the same conditions as above, the complex **3** was screened. Using DMAC as co-catalyst, the temperature was increased from 50 to 140 ^{o}C, which led to a reduction in the activity from 101,000 g/mmolV.h at 50 ^{o}C to 8,240 g/mmol.h at 110 ^{o}C; no activity was observed at 140 ^{o}C. The molecular weight decreased rapidly on oncreasing the temperature, whilst the PDI actually decreased from *ca.* 6 at 50 ^{o}C to a value in the region of 2 to 3 over the temperature range 80 – 110 ^{o}C, the same tedency as 1/DMAC/ETA. Results using DEAC were comparatively poorer, with the observed activity at 80 ^{o}C being about a tenth that observed when using **3**/DMAC/ETA; this system was inactive at 110 ^{o}C.

The activity displayed by **4** at 50 ^{o}C using DMAC as co-catalyst was similar to that observed for **3**, *i.e. ca.* 100,000 g/mmolV.h. The activity of **4** then decreased to about 49,700 g/mmolV.h at 80 ^{o}C, after which it rapidly dropped to about one tenth of this value at 110 ^{o}C, similar to that of **3**. M_ws for **4** are relatively higher than those of **1** and **3**, but the trends observed for the PDI were analogous to those observed for **1** and **3**. Use as DEAC as co-catalyst again afforded inferior activities to those observed when using DMAC, and there was less control over molecular weight upon DEAC/ETA activation. However, higher M_ws than those by DMAC/ETA activation resulted from the use of **1**, **3** and **4.** Despite the lowering of the observed activity at 110 ^{o}C (to 920), it was found to increase somewhat at 140 ^{o}C to 7,560 g/mmolV.h. Considering with the fact that PDI increases as the temperature raises, different active species from those at low temperature must be generated at 140 ^{o}C.

The melting points of the polyethylene obtained from systems employing **1**, **3** and **4** (and the standard catalyst) were all in the range 129.0 – 136.9 ^{o}C, consistent with the formation of linear polyethylene. NMR data for the polymers at the lower end of the melting point range did not show any evidence of branching. Therefore, it is suggested that low T_m is derived from low molecular weight polyethylene.

To benchmark the calixarene catalyst systems decribed above, the complex $VO(OEt)Cl_2$ was screened using both DMAC and DEAC as co-catalysts under the same conditions as above. Use of DMAC

afforded an activity of 74,720 g/mmolV.h at 50 ^{o}C, which dropped off only slightly (to 70,800 g/mmolV.h) on increasing the temperature to 80 ^{o}C. However, on further increasing the temperature to 110 ^{o}C, the activity fell away (down to 19,360 g/mmolV.h), which however is higher than observed for **3** (8,240 g/mmolV.h) and **4** (5,240 g/mmolV.h) at the same temperature, but lower than that observed for **1** (26,700 g/mmolV.h). In the case of DEAC, the activity observed at 50 ^{o}C was 96,700 g/mmolV.h, which halved at 80 ^{o}C (to 47,440 g/mmolV.h) and then fell off rapidly at 110 ^{o}C (17,340 g/mmolV.h) and 140 ^{o}C (3,560 g/mmolV.h); of the calixarene systems, only **1** exhibited any activity at 140 ^{o}C (*ca.* 7,500 g/mmolV.h). The general activity trends observed can be summarized as follows: for DMAC, at 50 ^{o}C, **1** > **3**, and **4** > $VO(OEt)Cl_2$; at 80 ^{o}C, **1** > $VO(OEt)Cl_2$, **3** > **4**; at 110 ^{o}C, **1** > $VO(OEt)Cl_2$ > **3**, **4**; at 140 ^{o}C, **4** > $VO(OEt)Cl_2$, **3**, **4**; for DEAC, at 50 ^{o}C, $VO(OEt)Cl_2$ > **1** > **3** > **4**; at 80 ^{o}C, $VO(OEt)Cl_2$ > **1**, **3** > **4**; at 110 ^{o}C, $VO(OEt)Cl_2$ > **1** > **3**, **4**; at 140 ^{o}C, **4** > $VO(OEt)Cl_2$ > **1**, **3**.

Co-polymerization of ethylene with propylene

The co-polymerization of ethylene with propylene was conducted in the presence of DMAC, DEAC or TMA at 50 ^{o}C over 30 mins. Results are presented in Table 5. For **1**, **3** and **4**, best results were obtained using DMAC as co-catalyst, with **1** achieving an activity of 65,100 g/mmolV.h and %C3 incorporation of 10.9 mol%. Use of DEAC as co-catalyst afforded lower molecular weights with %C3 in the range 7.1 – 8.2 mol%. However, results using TMA were disappointing (activity < 440 g/mmolV.h) and so further evaluation using this co-catalyst was discontinued.

In general, the activities of **1**, **3** and **4** were lower than $VO(OEt)Cl_2$, whilst the incorporation of propylene was 7.1 – 10.9 mol% was comparable (*cf* 10 mol% for $VO(OEt)Cl_2$). Within the calixarene series, the general activity trends observed can be summarized as follows: for DMAC, **1** > **3** > **4** and for DEAC, **1**, **3** > **4**.

Table 4. Ethylene polymerization results[a]

Run	Pre-Cat	Co-Cat	T[c]	Yield[b]	Activity[d]	M_w[e]	M_n[e]	PDI	T_m[f]
1	**$VO(OEt)Cl_2$**	DMAC	50	0.374	74,720	946,000	169,000	5.6	134.7
2			80	0.354	70,800	138,000	45,700	3.0	133.3
3			110	0.097	19,36				134.5
4			140	trace	-				
5		DEAC	50	0.483	96,700	317,000	56,800	5.6	134.4
6			80	0.237	47,440	209,000	27,200	7.7	134.0
7			110	0.087	17,340				133.8
8			140	0.018	3,560				128.9
10	**1**	DMAC	50	0.331	132,000	789,000	176,000	4.5	134.5
12			80	0.408	163,000	133,000	55,600	2.4	132.9
13			110	0.067	26,700	30,800	14,500	2.1	132.8
14			140	trace	-				
15		DEAC	50	0.184	73,500	554,000	115,000	4.8	131.6
16			80	0.015	6,080	316,000	12,300	25.7	132.0
17			110	0.011	4,400	112,000	5,710	19.5	130.4
18			140	trace	-				
19	**3**	DMAC	50	0.251	101,000	752,000	118,000	6.4	136.5
20			80	0.202	80,800	158,000	67,700	2.3	136.9
21			110	0.021	8,240	27,300	8,550	3.2	132.8
22			140	trace	-				
23		DEAC	50	0.149	59,400	663,000	126,000	5.3	132.1
24			80	0.021	8,480	375,000	37,600	10.0	133.0
25			110	trace	-				
26			140	trace	-				
27	**4**	DMAC	50	0.260	104,000	945,000	190,000	5.0	136.8
28			80	0.124	49,700	272,000	86,800	3.1	134.7
29			110	0.013	5,240				133.3
30			140	0.001	480				129.0
31		DEAC	50	0.081	32,200	941,000	153,000	6.2	129.6
32			80	0.009	3,440	491,000	20,500	24.0	133.4
33			110	0.002	920				130.7
34			140	0.019	7,560				132.1

[a] **Conditions**: 30 minutes, 5 mL toluene, 0.005 µmol V, 0.8 MPa ethylene, 20000 equivalents co-catalyst (v V), 20000 equivalents ETA (v V), reaction quenched with isobutylalcohol; [b] grams, [c] °C, [d] (g/(mmolV.hr)), [e] Determined by GPC, reported using polyethylene calibration, [f] °C polymer melting point.

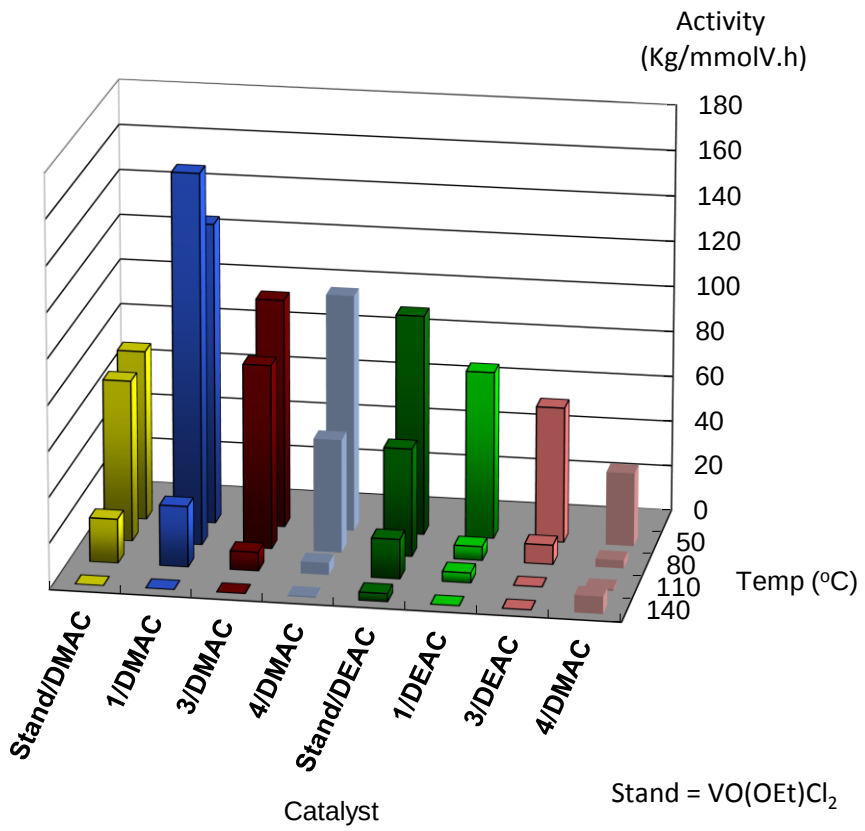

Figure 8. Activity in ethylene polymerization at 50 – 140 °C by $VO(OEt)Cl_2$, **1**, **3, and 4**.

Table 5. Ethylene/propylene co-polymerization results[a]

Run	Pre-Cat	Co-Cat	Yield[b]	Activity[c]	%C3[d]	M_w[e]	M_n[e]	PDI	T_m[f]
1	**$VO(OEt)Cl_2$**	DMAC	0.391	156,000	10.0	241,000	86,600	2.8	88.9
2		DEAC	0.191	76,400	9.1	75,700	42,700	1.8	90.2
3	**1**	DMAC	0.163	65,100	10.9	198,000	69,500	2.9	90.3
4		DEAC	0.070	28,000	8.2	105,000	53,000	2.0	91.9
5		Me_3Al	0.0005	200	-	-	-	-	-
6	**3**	DMAC	0.105	41,800	7.8	321,000	122,000	2.6	92.9
7		DEAC	0.071	28,200	7.8	88,700	46,800	1.9	93.7
8		Me_3Al	0.001	440	-	-	-	-	-
9	**4**	DMAC	0.063	25,000	7.9	264,000	120,000	2.2	92.3
10		DEAC	0.061	24,200	7.1	127,000	45,000	2.8	91.1

[a] **Conditions**: 5 mL toluene, 30 minutes, 50 °C, 0.005 µmol V, 0.4 MPa ethylene, 0.4 MPa propylene, 20000 equivalents co-catalyst (v V), 20000 equivalents ETA (v V), reaction quenched with isobutylalcohol; [b]grams, [c](g/(mmolV.hr)), [d] Mol% determined by FT-IR. [e] Determined by GPC, reported using polyethylene calibration, [f] °C polymer melting point.

Conclusion

In conclusion, use of the heterobimetallic complexes [MVO(O*t*Bu)$_4$] (M = Na, K), formed *in-situ* from $VOCl_3$ and MO*t*Bu, with p-*tert*-butylcalix[8]arene led to the formation of highly crystalline vanadium complexes, which adopt intriguing structural motifs (shallow saddle-shaped for **1** and **3**; pleated loop for **2**), often stabilized by the presence of alkali metal cations. In the case of lithium, it only proved possible to isolate crystalline products when the addition was reversed such that $VOCl_3$ was added to a pre-mixed solution of p-*tert*-butylcalix[8]arene and LiO*t*Bu. The products when using lithium contain, in the case of **4**, a central lantern-type cage capped top and bottom by an Li_2O_2 diamond with the calix[8]arene adopting a in a 'down, down, out, out, down, down, out, out' conformation, or a shallow saddle-shaped conformation (as in **5**).

For the polymerization of ethylene, using either DMAC or DEAC as co-catalyst and the re-activator ETA, the systems were all highly active, producing high molecular weight linear polyethylene. In most cases, activities were lower than the standard catalyst VO(OEt)Cl_2 though some properties of the calixarene systems proved noteworthy, namely the activity of **4** at 140 ^oC surpassed that of the benchmark catalyst and secondly, in some instances the calixarene-based systems gave products of higher molecular weight than VO(OEt)Cl_2 but with comparable activity, which may be an advantage for industrial use.

Experimental

General:

All manipulations were carried out under an atmosphere of dry nitrogen using conventional Schlenk and cannula techniques or in a conventional nitrogen-filled glove box. Diethyl ether and tetrahydrofuran were refluxed over sodium and benzophenone. Toluene was refluxed over sodium.

Dichloromethane and acetonitrile were refluxed over calcium hydride. All solvents were distilled and degassed prior to use. IR spectra (nujol mulls, KBr or NaCl windows) were recorded on a Nicolet Avatar 360 FT IR spectrometer; ^{1}H NMR spectra were recorded at room temperature on a Varian VXR 400 S spectrometer at 400 MHz or a Gemini 300 NMR spectrometer or a Bruker Advance DPX-300 spectrometer at 300 MHz. The ^{1}H NMR spectra were calibrated against the residual protio impurity of the deuterated solvent. Elemental analyses were performed by the elemental analysis service at the London Metropolitan University. The ligand $L^{8}H_8$ was prepared as described in the literature. [13] The precursors [V(NR)(O*t*Bu)$_3$] were prepared via K*t*OBu using the method of Maatta. [14] For the polymerization studies, the dry toluene employed as a polymerization solvent was purified by passage through columns of activated alumina and BASF R3-11 oxygen scavenger. Methylaluminoxane (MAO) was purchased from Albemarle Corporation as a 1.2 M toluene solution. This solution was dried under vacuum to remove the toluene and a substantial fraction of the $AlMe_3$, to produce "dried MAO " (DMAO). Ethylene was obtained from Sumitomo Seika Co.

Synthesis of [Na(NCMe)$_5$][(VO)$_2$L^{8}H]·4MeCN (**1**·4MeCN)

The salt [NaVO(O*t*-Bu)$_4$] (formed *in-situ* from $VOCl_3$ 0.27 cm^3, 2.89 mmol and NaO*t*-Bu 1.12 g, 11.65 mmol) and *p-tert*-butylcalix[8]areneH_8, $L^{8}H_8$ (1.87 g, 1.44 mmol) were refluxed in toluene (30 ml) for 12 h. Following removal of volatiles *in-vacuo*, the residue was extracted into hot (heat gun) acetonitrile (30 ml), affording **1** as brown blocks on prolonged standing (1 -2 days) at ambient temperature. Yield: 1.23 g, 47 %; elemental analysis (sample dried *in-vacuo* for 12 h) calculated for **1**·4CH_3CN – 5MeCN, $C_{96}H_{117}N_4NaO_{10}V_2$: C 71.5, H 7.3, N 3.5 %; found: C 70.5, H 6.8, N 3.5 % [15]; IR (nujol mull, KBr): 3176w, 2263w, 1733w, 1610w, 1293s, 1260s, 1203s, 1153m, 1093s, 1018s, 967s, 911m, 869m, 808s, 722s, 670w, 633w, 581w, 572w, 553w, 534w, 521w, 464w, 448w, 430w. MS (ESI): *m/z* 1589 [M]$^+$ Na(NCMe)$_5$. ^{1}H NMR ($CDCl_3$, 400MHz): 15.49 (Br, s, O-H-O, 1H) 7.30 (s, 4H, aryl*H*), 7.21 (s, 6H,

aryl*H*), 7.17 (s, 2H, aryl*H*), 7.06 (s, 2H, aryl*H*), 6.97 (s, 2H, aryl*H*), 5.97 (d, 2H, $^{2}J_{HH}$ = 12.6 Hz, *endo*-CH_2), 5.66 (d, 4H, $^{2}J_{HH}$ = 13.7 Hz, *endo*-CH_2), 4.66 (d, 2H, $^{2}J_{HH}$ = 11.8 Hz, *endo*-CH_2), 3.54 (d, 2H, $^{2}J_{HH}$ = 13.5 Hz, *exo*-CH_2), 3.49 (d, 2H, $^{2}J_{HH}$ = 12.3 Hz, *exo*-CH_2), 3.38 (d, 2H, $^{2}J_{HH}$ = 13.7 Hz, *exo*-CH_2), 3.30 (d, 2H, $^{2}J_{HH}$ = 11.8 Hz, *exo*-CH_2), 1.30 (overlapping s, 72H, C(CH_3)$_3$) ^{51}V NMR ($CDCl_3$) δ: –202.4 ($\omega^1/_2$ 700 Hz), –333.8 ($\omega^1/_2$ 500 Hz).

Synthesis of {[(Na(VO)$_4$L^8)(Na(NCMe))$_3$] [Na(NCMe)$_6$]}$_2$·10MeCN (**2**·10MeCN)

As for **1**, but using [NaVO(O*t*-Bu)$_4$] ([$VOCl_3$] 0.27 cm^3, 2.89 mmol and NaO*t*-Bu 1.12 g, 11.65 mmol) and L^{8}H$_8$ (0.93 g, 0.72 mmol), affording **2** as yellow blocks. Yield: 0.57 g, 17 %; elemental analysis calculated for **5**·10 CH_3CN, $C_{212}H_{262}N_{18}Na_8O_{32}V_8$·10 C_2H_3N: C 60.9, H 6.4, N 8.6 %; found: C 61.0, H 6.5, N 8.5 %; IR (nujol mull, KBr): *v* 2320w, 1604w, 1300w, 1261s, 1204w, 1094bs, 1019bs, 916w, 866w, 800s, 722m, 702w, 660w; MS (solvent free MALDI, DCTB matrix) *m/z*: 3200 (M^+ – 10MeCN – 2Na(MeCN)$_6$ – 2Na(MeCN)$_3$ – 3Na – VO), 3159 (M^+ – 11MeCN – 2Na(MeCN)$_6$ – 2Na(MeCN)$_3$ – 3Na – VO). ^{1}H NMR ($CDCl_3$, sample dried for 12 h) δ: 7.25 (m, 4H, aryl*H*), 7.23 (m, 6H, aryl*H*), 7.18(m, 4H, aryl*H*), 7.09 (br s, 6H, aryl*H*), 7.06 (m 4H, aryl*H*), 7.05 (d, 4H, J_{HH} = 1.50 Hz, aryl*H*), 7.02 (br s, 2H, aryl*H*), 6.94 (m, 2H, J_{HH} = 1.99 Hz, aryl*H*), 6.15 (d, $^{2}J_{HH}$ 14.5 Hz, 2H, *endo*-CH_2), 5.36 (d, $^{2}J_{HH}$ 14.0 Hz, 4H, *endo*-CH_2), 5.15 (d, $^{2}J_{HH}$ 13.0 Hz, 4H, *endo*-CH_2), 4.62 (overlapping d, J obscured, 4H, *endo*-CH_2), 4.38 (d, $^{2}J_{HH}$ 13.2 Hz, 2H, *endo*-CH_2), 3.64 (d, $^{2}J_{HH}$ 14.5 Hz, 2H, *exo*-CH_2), 3.54 (d, $^{2}J_{HH}$ 14.2 Hz, 2H, *exo*-CH_2), 3,43 (d, $^{2}J_{HH}$ 12.1 Hz, 2H, *exo*-CH_2), 3.24 (d, J obscured, 2H, *exo*-CH_2), 3.23 (d, $^{2}J_{HH}$ 14.0 Hz, 4H, *exo*-CH_2), 2.98 (d, $^{2}J_{HH}$ 13.2 Hz, 2H, *exo*-CH_2), 2.84 d, $^{2}J_{HH}$ 13.0 Hz, 2H, *exo*-CH_2), 1.24 (s, 18H, C(CH_3)$_3$), 1.21 (s, 36H, C(CH_3)$_3$), 1.18 (s, 18H, C(CH_3)$_3$), 1.05 (s, 18H, C(CH_3)$_3$), 1.03 (s, 36H, C(CH_3)$_3$), 1.01 (s, 18H, C(CH_3)$_3$). ^{51}V NMR (105.1 MHz, $CDCl_3$) δ: -481.2 ($\omega^1/_2$ 585 Hz).

Synthesis of $[(VO)_4L^8(\mu^3\text{-}O)_2]\cdot 3MeCN$ and $\mathbf{3}\cdot 3CH_2Cl_2$

As for **1**, but using $[VO(O\textit{t}\text{-}Bu)_3]$ ($VOCl_3$ 0.27 cm^3, 2.89 mmol and KO*t*-Bu 1.03 g, 8.67 mmol) and L^8H_8 (0.93 g, 0.72 mmol), affording $\mathbf{6}\cdot 3CH_3CN$ as black blocks. Yield: 0.47 g, 38 %; elemental analysis calculated for $\mathbf{3}\cdot 3CH_3CN$ $C_{88}H_{104}V_4O_{14}.3C_2H_3N$: C 65.9, H 6.7, N 2.5 %; found: C 65.7, H 6.3, N 3.2 %; IR (nujol mull, cm^{-1}, KBr): 1594w, 1567w, 1303w, 1288w, 1260s, 1226w, 1201m, 1172w, 1098bs, 1022s, 944w, 913w, 875m, 833m, 794s, 734w, 705w, 670w, 653m, 642w, 617w, 574w. MS: (MALDI): $[MH^+]$ 1589.6 (solvent free) *m/z*, 1529.5 $[MH^+]$ – VO, 1488.5 $[MH^+]$ – 2V. ^{1}H NMR (C_6D_6, sample dried for 12 h) δ: 7.34 – 6.96 (overlapping m, 16H, Aryl*H*), 5.05 (d, $^2J_{HH}$ 11.7 Hz, 2H, *endo*-C*H*$_2$), 4.89 $^2J_{HH}$ 14.4 Hz, 4H, *endo*-C*H*$_2$), 4.29 $^2J_{HH}$ 12.6 Hz, 2H, *endo*-C*H*$_2$), 3.14 (d, $^2J_{HH}$ 12.6 Hz, 2H, *exo*-C*H*$_2$), 2.98 – 2.92 (overlapping m, J obscured, 4H, *exo*-C*H*$_2$), 2.55 (d, $^2J_{HH}$ 14.4 Hz, 2H, *exo*-C*H*$_2$), 0.95 (s, 36H, C(C*H*$_3$)$_3$), 0.74 (s, 36H, C(C*H*$_3$)$_3$), 0.28 (s, 3H *Me*CN). ^{51}V NMR ($CDCl_3$) δ: –209.7 ($\omega^1/_2$ 750 Hz), –341.1 ($\omega^1/_2$ 415 Hz). Re-crystallization of the crude product from dichloromethane afforded dark green rod-like crystals of $\mathbf{3}\cdot 3CH_2Cl_2$. Yield: 0.41 g, 31 %; elemental analysis calculated for $\mathbf{3}\cdot 3CH_2Cl_2$: $C_{88}H_{104}V_4O_{14}$ (solvent free): C 59.3, H 6.0; found: C 59.4, H 5.9 %; ^{51}V NMR ($CDCl_3$) δ: –213.6 ($\omega^1/_2$ 1500 Hz), –341.2 ($\omega^1/_2$ 330 Hz), –371.2.

Synthesis of $\{(VO_2)_2Li_6[L^8](thf)_2(O\textit{t}Bu)_2(Et_2O)_2\}\cdot Et_2O$ ($\mathbf{4}\cdot Et_2O$)

To L^8H_8 (1.00 g, 0.77 mmol) in THF/Et_2O (1:1; 30 ml) was added a solution of LiO*t*Bu (8.01 ml, 1.0 M, 8.01 mmol) at ambient temperature and stirred for 2 h. The system was then cooled to –78 ^{o}C and $VOCl_3$ (0.15 ml, 1.59 mmol) was slowly added and the system was allowed to warm to ambient temperature and stirred for 12 h. Filtration and concentration to about two thirds the volume afforded orange prisms on prolonged standing at 0 ^{o}C. Yield: 0.74 g, 44.0 %; elemental analysis calculated for $\mathbf{4}\cdot Et_2O$ $C_{112}H_{160}Li_6O_{22}V_4\cdot(C_4H_8O)$: C 64.0, H 7.9 %; found: C 63.7, H 7.8 %; IR (nujol mull, cm^{-1},

NaCl): 1599w, 1573w, 1414w, 364m, 1303w, 1290w, 1259s, 1202w, 1184w, 1093bs, 1020bs, 944w, 893w, 880w, 867w, 799s, 722w, 687w, 670w, 625w, 613w, 595w, 570w, 549w, 536w. MS (EI positive mode) *m/z*, 2101.8 [M^+] – Et_2O, 1885.5 [M^+] – Et_2O – THF, 1774.6 [M^+] – Et_2O – THF – 5Li; ^{1}H NMR ($CDCl_3$) δ: 7.28 – 6.95 (overlapping m, 16H, aryl*H*), 4.63 (d, 2H, $^2J_{HH}$ 12.0 Hz, *endo*-CH_2), 4.35 (overlapping d, 6H, *endo*-CH_2), 3.86 and 3.66 (2x bs, 20H, OCH_2 of 3x Et_2O, 2x THF), 3.47 (d, 2H, $^2J_{HH}$ 16.0 Hz, *exo*-CH_2), 3.39 (d, 2H, $^2J_{HH}$ 12.0 Hz, *exo*-CH_2), 3.34 (d, 4H, $^2J_{HH}$ 12.0 Hz, *exo*-CH_2), 1.78 (bs, 8H, CH_2 of 2x THF), 1.52 (s, 18H, OC(CH_3)$_3$), 1.48 (s, 72H, C(CH_3)$_3$), 1.25 (overlapping m, 18H, OCH_2CH_3 of 3x Et_2O). ^{51}V NMR ($CDCl_3$) δ: –672.1, –694.0.

Synthesis of [Li(NCMe)$_4$][$(VO)_2L^8H$]·8MeCN (**5**·8MeCN)

As for **4**, but following removal of THF, the residue was extracted into hot MeCN (30 ml). Yield: 1.02g, 68.9 %; elemental analysis calculated for **5**·8MeCN $C_{88}H_{105}O_{10}V_2^-\cdot C_8H_{12}LiN_4^+\cdot 8(C_2H_3N)$: C 69.9, H 7.4, N 8.7 %; found: C 69.3, H 7.2, N 8.5 %; IR (nujol mull, cm^{-1}, NaCl): 1573w, 1453s, 1415s, 1316s, 1292s, 1260s, 1201s, 1116s, 1094s, 1023s, 966s, 911m, 869m, 834m, 818s, 806s, 780m, 750m, 725m, 673w, 634w. MS (ESI): 1923 (M^+ – H), 1876 (M^+ – Li – MeCN), 1712 (M^+ – Li – 5MeCN), 1630 (M^+ – Li – 7MeCN), 1589 (M^+ – Li – 8MeCN), 1548 (M^+ – Li – 9MeCN), 1507 (M^+ – Li – 10MeCN), 1425 (M^+ – Li – 12MeCN). ^{1}H NMR (CD_3CN, sample dried for 12 h) δ: 7.33 (m, J_{HH} 4.0 Hz, 2H, *arylH*), 7.26 (overlapping m, 4H, *arylH*), 7.23 (overlapping m, 2H, *arylH*), 7.20 (m, J_{HH} 4.0 Hz, 2H, *arylH*), 7.18 (m, J_{HH} 4.0 Hz, 2H, *arylH*), 7.00 (m, J_{HH} not observed, 2H, *arylH*), 6.94 (m, J_{HH} 4.0 Hz, 2H, *arylH*), 5.82 (2x overlapping doublets, $^2J_{HH}$ 12.0 Hz, 2H, *endo*-CH_2), 5.48 (2x overlapping doublets, $^2J_{HH}$ 12.0 Hz, 2H, *endo*-CH_2), 5.40 (2x overlapping doublets, $^2J_{HH}$ 14.0 Hz, 2H, *endo*-CH_2), 4.50 (2x overlapping doublets, $^2J_{HH}$ 12.0 Hz, 2H, *endo*-CH_2), 3.45 (2x overlapping doublets, $^2J_{HH}$ 12.0 Hz, 2H, *exo*-CH_2), 3.38 (4x overlapping doublets, $^2J_{HH}$ obscurred, 4H, *exo*-CH_2),

3.23 (2x overlapping doublets, $^2J_{HH}$ 12.0 Hz, 2H, *exo*-CH_2), 1.97 (s, 24H, *Me*CN), 1.96 (s (partially obscurred by CD_3CN, 12H, MeCN), 1.26 – 1.24 (overlapping s, 54H, C(CH_3)$_3$), 1.21 – 1.20 (2x s, 18H, C(CH_3)$_3$), O*H* not observed.

Synthesis of [*t*-BuNH_3]{[V(*p*-tolylN)]$_2$L^{8}H}·3½MeCN (**6**·3½MeCN)

[V(*t*-BuN)(O*t*-Bu)$_3$] (0.5 g, 1.46 mmol) and [V(*p*-tolylN)(O*t*-Bu)$_3$] (0.55 g, 1.46 mmol) in toluene (30 cm^3) were stirred at ambient temperature for 3 h. L^{8}H$_8$ (1.90 g, 1.46 mmol) was added, and the system was refluxed for 6 h, after which volatiles were removed *in-vacuo* and the residue was extracted into warm MeCN (30 cm^3). Prolonged standing at ambient temperature afforded orange/brown plates of **6**, Yield: 0.71 g, 26 %. Further cooling to –20 ^{o}C afforded further crops of **6** along with a highly solvent dependant brown solid. elemental analysis calculated for **6**·3½ CH_3CN, $C_{113}H_{141.5}N_{6.5}V_2O_8$: C 74.5, H 7.8, N 5.0 %; found: C 73.7, H 7.4, N 4.5 %; IR (nujol mull, KBr, cm^{-1}): 2078w, 1594w, 1419w, 1402w, 1302w, 1261s, 1200m, 1097bs, 1022s, 912w, 872w, 832m, 795s, 726w, 705w, 669w, 653w, 642w, 613w, 574w, 558w, 532w, 450w. ^{1}H NMR ($CDCl_3$, sample dried *in-vacuo* for 1 h) δ: 8.35 (br s, *t*BuNH_3), 7.30 – 6.92 (overlapping m, 24H, aryl *H*), 4.80 (d, $^2J_{HH}$ 12.0 Hz, 2H, *endo*-CH_2), 4.61 (bm, 2H, *endo*-CH_2), 4.35 (bm, 2H, *endo*-CH_2), 4.22 (d, $^2J_{HH}$ 12.0 Hz, 2H, *endo*-CH_2), 3.39 (d, $^2J_{HH}$ 11.6 Hz, 2H, *exo*-CH_2), 3.29 (bm, 2H, *exo*-CH_2), 3.12 (d, $^2J_{HH}$ 12.0 Hz, 2H, *exo*-CH_2), 3.01 (bm, 2H, *exo*-CH_2), 2.35 (s, 6H, CH_3C$_6$H$_4$), 2.00 (s, 6H, MeCN), 1.48, 1.34, 1.24, 1.14 (4x s, 72H, C(CH_3)$_3$), O*H* not observed.

Polymer Characterization

The melt transition temperatures (T_m) of the polyethylene (PE) and ethylene/propylene copolymer (EPR) were determined by differential scanning calorimetry (DSC) with a Shimadzu DSC-60 instrument. The polymer samples were heated at 50 ^{o}C/min from 20 ^{o}C to 200 ^{o}C, held at 200 ^{o}C for 5

min, and cooled to 0 ^{o}C at 20 ^{o}C/min. The samples were held at this temperature for 5 min, and then reheated to 200 ^{o}C at 10 ^{o}C/min. The reported T_m was determined from the second heating scan unless otherwise noted.

Molecular weights (M_w and M_n) and polymer disparity index (PDI) of PE and EPR were determined using a Waters GPC2000 gel permeation chromatograph equipped with four TSKgel columns (two sets of TSKgelGMH$_6$-HT and two sets of TSKgelGMH$_6$-HTL) at 140 ^{o}C using polystyrene calibration. *o*-Dichlorobenzene (ODCB) was used as the solvent.

The propylene content of the EPR was measured by IR analysis using a JASCO FT-IR.

Polymerization Procedure

Polymerization reactions were performed in a parallel pressure reactor (Argonaut Endeavor® Catalyst Screening System) containing 8 reaction vessels (15 mL) each equipped with a mechanical stirrer and monomer feed lines. At first, a toluene solution (and a toluene solution of ETA as necessary) was injected into each vessel. *For ethylene polymerization*, the solution was heated to the polymerization temperature (T_p) and thermally equilibrated, and the nitrogen atmosphere was replaced with ethylene and the solution was saturated with ethylene at the polymerization pressure. *For ethylene/propylene copolymerization*, the nitrogen atmosphere was replaced with propylene and the reaction vessels were pressurized with propylene (0.4 MPa at 25 ^{o}C), and the solution was heated to the T_p and thermally equilibrated, then ethylene was introduced into the reactor up to the polymerization pressure. *In all cases* the polymerization was started by addition of a toluene solution of alkyl aluminum or alkyl aluminum chloride followed by addition of a toluene solution of the vanadium complex (0.50 mL toluene solution of complex followed by 0.25 mL toluene wash). The total volume of the reaction mixture was 5 mL for all polymerizations. The pressure was kept constant by feeding ethylene on demand. After the reaction, the polymerization was stopped by addition of

excess isobutyl alcohol. The resulting mixture was added to acidified methanol (45 ml containing 0.5 ml of concentrated HCl). The polymer was recovered by filtration, washed with methanol (2 × 10 ml) and dried in a vacuum oven at 80 ^{o}C for 10 h.

Crystallography

This set of structures were particularly challenging, so we describe here the details of how the various problems were approached. Crystal data were collected on a Bruker SMART 1000 CCD diffractometer using narrow slice 0.3° ω-scans for **6**·3½MeCN**, (**Bruker APEX 2 for **1**·4MeCN, **2**·10MeCN, **3**·3MeCN, **3**·3CH_2Cl_2, and **5**·8MeCN **)**. [16] Data for **5**·10MeCN, **3**·3MeCN, and **3**·3CH_2Cl_2 were collected at Daresbury Laboratory SRS Station 9.8 using silicon 111 monochromated X-radiation due to small crystal size or weak diffraction [17]. Data for **4**·Et_2O was collected on a Rigaku AFC12 Saturn 724+ Kappa CCD diffractometer using a rotating anode source. [18] Data were corrected for Lp effects and for absorption, based on repeated and symmetry equivalent reflections [16, 17], and solved by direct methods [19, 20]. Structures were refined by full matrix least squares on F^2 [19, 20]. H atoms were included in a riding model except for H(5) in **1**·4MeCN, H(2) and H(6) in **5**·8MeCN, and H(7) in **6**·3½MeCN for which coordinates were freely refined. Hydrogen atom U_{iso} values were constrained to be 120 % of that of the carrier atom except for methyl, ammonium, and hydroxyl-H (150 %). Several structures exhibited two-fold disorder in, *tert*-butyl groups and/or solvent molecules where restraints were applied to geometry and anisotropic displacement parameters. Some solvent molecules were diffuse and refined at half weight so numbers of solvent molecules of crystallisation should be regarded as approximate. Structures **3**·3MeCN and **3**·3CH_2Cl_2 are isomorphous and are two-component twins related via a 180° rotation about reciprocal axis [0 1 0]. The major component was 56.80(16) % in the case of the former. Structure **3**·3MeCN was best treated using the diffraction intensities from

both twin components, while for **3**·3CH_2Cl_2 approximately detwinned diffraction data were used. The badly disordered third CH_2Cl_2 in **3**·3CH_2Cl_2, three acetonitriles in **2**·10MeCN, and the Et_2O in **4**·Et_2O were modelled as regions of diffuse electron density by the Platon Squeeze procedure. [21] Twinning is suspected in structures **2**·10MeCN and **4**·Et_2O, and **5**·8MeCN but no satisfactory twin model could be developed. Further details are provided in Table 6. CCDC 895364 – 895369 and 1017370-1017371 contain the supplementary crystallographic data for this paper. These data can be obtained free of charge from The Cambridge Crystallographic Data Centre via www.ccdc.cam.ac.uk/data_request/cif.

Acknowledgements

The EPSRC and STFC are thanked for financial support (including an Overseas Travel grant to CR) and the award of beamtime at Daresbury Laboratory (Station 9.8). Drs Simon J. Coles, John E. Warren and Pierre J. Rizkallah are thanked for technical support at Daresbury Laboratory. The EPSRC Mass Spectrometry Service (Swansea, UK) and the EPSRC National X-ray Crystallographic Service (Southampton) are thanked for data collection.

Supporting Information Available: X-ray crystallographic files CIF format for the structure determinations of compound **1 – 6**.

Table 6. Crystallographic data for complex **1**·4MeCN, **2**·10MeCN, **3**·3MeCN and **3**·3CH_2Cl_2

Compound	**1**·4(CH_3CN)	**2**·10(CH_3CN)	**3**·3(CH_3CN)	**3**·3(CH_2Cl_2)
Formula	$C_{98}H_{120}V_2N_5NaO_{10}\cdot 4CH_3CN$	$C_{212}H_{262}V_8N_{18}Na_8O_{32}\cdot 10CH_3CN$	$C_{88}H_{104}V_4O_{14}\cdot 3CH_3CN$	$C_{88}H_{104}V_4O_{14}\cdot 3CH_2Cl_2$
Formula weight	1817.08	4576.38	1712.63	1844.25
Crystal system	monoclinic	monoclinic	triclinic	triclinic
Space group	$P2_1/n$	$P2_1/n$	$P\bar{1}$	$P\bar{1}$
Unit cell dimensions				
a (Å)	12.4731(7)	20.8729(9)	13.763(6)	13.870(2)
b (Å)	31.3969(17)	21.4271(9)	18.382(8)	18.180(3)
c (Å)	27.8042(15)	30.0519(12)	18.985(8)	18.983(3)
α (º)	90	90	74.641(6)	75.296(2)
β (º)	102.8887(8)	103.6628(18)	86.251(6)	86.178(2)
γ (º)	90	90	79.451(7)	77.749(2)
V (Å^3)	10614.2(10)	13060.2(9)	4553(3)	4524.0(13)
Z	4	2	2	2
Temperature (K)	150(2)	150(2)	150(2)	150(2)
Wavelength (Å)	0.71073	0.6939	0.6884	0.6911
Calculated density (g.cm^{-3})	1.137	1.164	1.249	1.354
Absorption coefficient (mm^{-1})	0.238	0.352	0.460	0.638
Transmission factors (min./max.)	0.900 and 0.939	0.881 and 0.924	0.918 and 0.991	0.852 and 0.975
Crystal size (mm^3)	0.45 × 0.28 × 0.27	0.37 × 0.30 × 0.23	0.19 × 0.07 × 0.02	0.26 × 0.05 × 0.04
θ(max) (°)	27.2	24.0	24.0	26.7
Reflections measured	99178	110060	57516	71017
Unique reflections	23497	22011	15616	20773
R_{int}	0.0832	0.0973	0.1565	0.0921
Reflections with $F^2 > 2\sigma(F^2)$	14780	14349	8595	15274
Number of parameters	1320	1512	1114	1058
R_1 [$F^2 > 2\sigma(F^2)$]	0.0609	0.1156	0.0829	0.0932
wR_2 (all data)	0.1905	0.2870	0.2291	0.2706
GOOF, S	1.038	1.315	0.970	1.066

Largest difference peak and hole (e Å^{-3})	1.060 and –0.535	1.495 and –0.523	0.738 and –0.814	3.393 and –1.442

Table 6 con't. Crystallographic data for complex **4**·Et_2O, **5**·8MeCN and **6**·3½MeCN.

Compound	**4**.Et_2O	**5**.8MeCN	**6**·3½(CH_3CN)
Formula	$C_{112}H_{160}V_4O_{22}Li_6{\cdot}Et_2O$	$C_{88}H_{105}V_2O_{10}{\cdot}C_8H_{12}LiN_4{\cdot}8CH_3CN$	$C_{106}H_{131}V_2N_3O_8{\cdot}3½CH_3CN$
Formula weight	2175.89	1924.18	1820.71
Crystal system	monoclinic	triclinic	triclinic
Space group	*C*2/*c*	*P*$\bar{1}$	*P*$\bar{1}$
Unit cell dimensions			
a (Å)	33.361(16)	12.519(3)	12.2630(13)
b (Å)	12.011(5)	16.085(3)	16.9231(17)
c (Å)	32.820(14)	29.079(6)	27.809(3)
α (º)	90	80.780(3)	103.9105(18)
β (º)	116.34(4)	85.871(3)	100.1796(19)
γ (º)	90	73.333(3)	93.2503(18)
V (Å^3)	11786(10)	5535(2)	5484.2(10)
Z	4	2	2
Temperature (K)	100(2)	150(2)	150(2)
Wavelength (Å)	0.71073	0.71073	0.71073
Calculated density (g.cm^{-3})	1.226	1.155	1.103
Absorption coefficient (mm^{-1})	0.373	0.229	0.225
Transmission factors (min./max.)	0.964 and 0.987	0.849 and 0.966	0.869 and 0.991
Crystal size (mm^3)	0.10 × 0.07 × 0.04	0.74 × 0.31 × 0.15	0.64 × 0.11 × 0.04
θ(max) (°)	27.5	28.5	25.0
Reflections measured	47065	74023	36900
Unique reflections	13465	27412	18857
R_{int}	0.0553	0.1004	0.0834
Reflections with $F^2 > 2\sigma(F^2)$	9918	15246	8410
Number of parameters	782	1392	1201
R_1 [$F^2 > 2\sigma(F^2)$]	0.0872	0.0860	0.0734
wR_2 (all data)	0.2686	0.2288	0.2441
GOOF, *S*	1.051	1.042	0.979
	0.836 and –0.896	1.143 and –0.720	0.680 and –0.367

Largest difference peak and hole (e $Å^{-3}$)	

References

1. D. M. Homden and C. Redshaw, *Chem. Rev.*, **2008**, 108, 5086.

2. L. Giannini, A. Caselli, E. Solari, C. Floriani, A. Chiesi-Villa, C. Rizzoli, N. Re, A. Sgamellotti, *J. Am. Chem. Soc*. 1997, 119, 9198.

3. a) C. Redshaw, *Coord. Chem. Rev*., 2003, 244, 45. (b) The Chemistry of Metal Phenolates. Ed. Jacob Zabicky, Publisher Wiley, Y. Li, K.-Q. Zhao, C. Redshaw, A. Y. Nuñez, B. A. M. Ortega, S. Memon and T. A. Hanna, **2014**, ISBN:978-0-470-97358-5.

4. For recent examples, see a) R.D. McIntosh, S.M. Taylor, S. Sanz, C.M. Beavers, S.J. Teat, E.K. Brechin and S.J. Dalgarno, *Dalton Trans*. 2011, *40*, 12265 and references therein.

5. a) S. Singh and H. W. Roesky, *Dalton Trans.*, 2007, 1360. b) M. P. Weberski, Jr, C. Chen, M. Delferro, and T. J. Marks, *Chem. Eur. J.* 2012 **18**, 10715. c) M. Delferro, and T. J. Marks, *Chem. Rev*. 2011, **111** (3), 2450–2485.

6. (a) E. Hoppe, C. Limberg and B. Ziemer, *Inorg. Chem*., 2006, **45**, 8308. (b) E. Hoppe, C. Limberg, B. Ziemer and C. Mügge, *J. Mol. Cat A: Chem*., 2006, 251, 34. (c) C. Limberg, *Eur. J. Inorg. Chem.*, 2007, 3303.

7. (a) V.C. Gibson, C. Redshaw and M.R.J. Elsegood, *J. Chem. Soc., Dalton Trans*., 2001, 767. (b) C. Redshaw, M. A. Rowan, L. Warford, D. M. Homden, A. Arbaoui, M. R. J. Elsegood, S. H. Dale, T. Yamato, C. P. Casas and S. Matsui, *Chem. Eur. J.*, 2007, **13**, 1090. (c) L. Clowes, C. Redshaw and D.L. Hughes, *Inorg. Chem*. 2011, **50**, 7838. (d) C. Redshaw, L. Clowes, D.L. Hughes, M.R.J. Elsegood and T. Yamato, *Organometallics* 2011, **30**, 5620.

8. C. Redshaw, D. Homden, D. L. Hughes, J. A. Wright and M. R. J. Elsegood, *Dalton Trans*. **2009**, 1231-1242.

9. A. Arbaoui, C. Redshaw, M. R.J. Elsegood, V. E. Wright, A. Yoshizawa and T. Yamato, *Chem. Asian J*. **2010** *5*, 621.

10. C. Redshaw, M.J. Walton, K. Michiue, Y. Chao, A. Walton, P. Elo, V. Sumerin, C. Jiang and M.R.J. Elsegood, manuscript in preparation.

11. M. Bochmann, G. Wilkinson, G. B. Young, M. B. Hursthouse, K. M. A. Malik, *J. Chem. Soc., Dalton Trans.* **1980**, 1863.

12. (a) G.E. Hofmeister, F.E. Hahn and S.F. Pedersen, *J. Am. Chem. Soc*., 1989, 111, 2318. (b) G.E. Hofmeister, E. Alvarado, J.A. Leary, D.I. Yoon and S.F. Pedersen, *J. Am. Chem. Soc*., 1990, 112, 8843.

13. A. Arduini, A. Casnati in Macrocycle Synthesis (Ed.: D. Parker), Oxford University Press, 1996, chap. 7.
14. D. D. Devore, J. D. Lichtenhan, F. Takusagawa and E. A. Maatta, *J. Am. Chem. Soc.*, 1987, **109**, 7408.
15. The problems associated with calixarene microanalysis are well documented, for example, C. Redshaw, D. Homden, D.L. Hughes, J.A. Wright and M.R.J. Elsegood, *Dalton Trans*, 2009, 1231.
16. SMART (2001), SAINT (2001 & 2008&12), and APEX 2 (2008&12) software for CCD diffractometers. Bruker AXS Inc., Madison, USA.
17. (a) W. Clegg, M. R. J. Elsegood, S. J. Teat, C. Redshaw and V. C. Gibson, *J. Chem. Soc., Dalton Trans.*, 1998, 3037.
18. Rigaku Crystal Clear-SM Expert 3.1 b24 (2012) software for Diffractometers, Rigaku Corp.
19. G.M. Sheldrick, SHELXTL user manual, version 6.10. Bruker AXS Inc., Madison, WI, USA, (2000).
20. G.M. Sheldrick, (2008), *Acta Crystallogr*. **A64**, 112-122.
21. A.L. Spek, (1990), *Acta Crystallogr*. A46, C34.